A New Design for Cubic Spatially Processed Wideband Arrays

Mohammad Ghavami
London South Bank University
School of Engineering
103 Borough Road, London SE1 0AA, UK

Abstract

This paper presents a simple and novel formulation for the design and analysis of a generic cubic array with a single real coefficient for each antenna element, to steer the developed beam toward a certain desired angle in both azimuth (totally 360°) and elevation (totally 180°) directions. This configuration demonstrates frequency invariance of the directional patterns of the array within a relatively large fractional bandwidth which makes this array a potential candidate for wideband and ultra wideband applications. The required real coefficients are calculated based on matrix manipulation methods. However, the dimension of the matrices and vectors used in the computations are much less than the total number of antenna elements. Computer simulation shows the performance of the array with respect to the resolution of the main beam and frequency independence of the patterns and also in terms of the complexity and frequency range. Moreover, we will present a comparison between the proposed algorithm and the Fourier transform based methods and adaptive least mean square algorithm.

1 Introduction

Wideband beam formation has attracted interest due to its potential applications in different areas such as radar, medical imaging and telecommunications [1][2]. In conventional wideband beamforming methods that use both time and space domains, the wideband characteristics of the array is realized by applying the received signal of each antenna element to a predesigned set of adjustable filters [3] or pure time delays [4]. In some other

approaches which do not employ time-domain filters or delay elements, only a single real-values coefficient is used for each antenna element [5].

Distributed beamforming methods using three dimensional volumetric arrays present higher flexibility in terms of throughput and bandwidth. In the analysis presented in [6] different array topologies including cubic configuration have been considered. As expected, this work concludes that larger volumes of omnidirectional elements produce narrower radiation patterns. As an application of cubically located sensor arrays, the detection of a far field particle source has been studied in [7]. In another investigation, a cubic scanning array of antenna elements have been modelled and simulated. The behaviour of the resultant array is compared with the multiple planar array structure [8].

Cubic antenna arrays for wideband beamforming in both full azimuth and elevation directions using purely spatial processing has rarely been discussed in literature. In the method described in [1] and [9], Fourier transform techniques have been used to calculate the weights connected to each element. In another approach, steerable cubic antenna arrays are designed by optimization of the amplitude and phase excitations across the elements [10]. The novelty of this method is the application of an evolutionary optimization algorithm to a design problem.

In this paper a new algorithm is proposed to calculate the real multipliers of a linear cubic array. The main advantage of this method is the simplicity of the computation which does not involve two dimensional Fourier transform normally used in wideband array calculations. Moreover, it covers 360° of azimuth and 180° of elevation angles with a single structure. We also notice that the proposed method is superior in terms of overall size and frequency independence compared to the distributed technique presented in [6] which is using both temporal and spatial signal processing methodology. To compare our method with [7], we observe that in this reference the frequency dependence of the beam patterns is not taken into account during the design process. This lack of discussion on the frequency dependency of the phased array is also a drawback of the method presented in [8].

The rest of this paper is organized as follows. In section 2 we will introduce the cubic array formulation. Section 3 explains the design of coefficients. Section 4 presents some computer simulation results including a comparison between the proposed algorithm and two dimensional Fourier transform method of [9] and adaptive least mean square (LMS) algorithm [11]. Finally, section 5 concludes the paper.

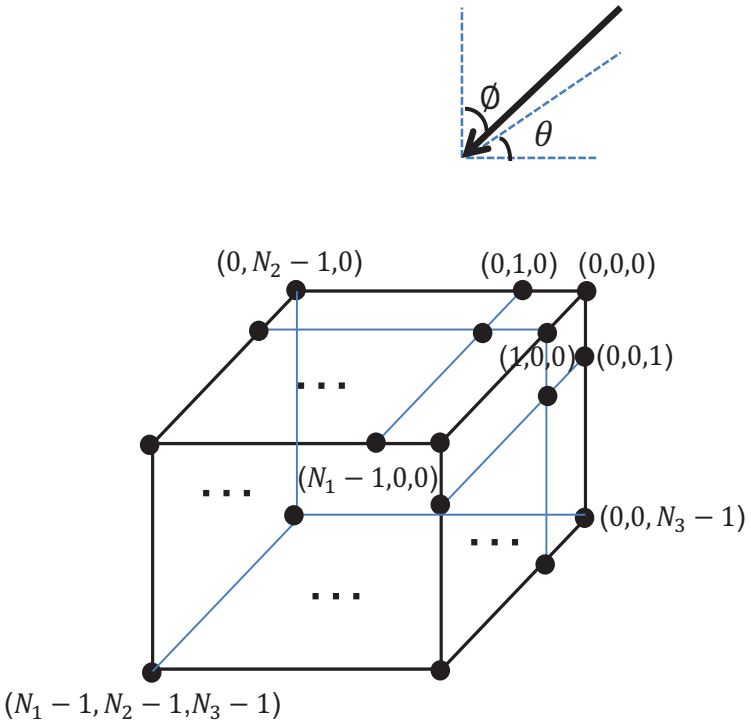

Figure 1: Location of the antenna elements on the cubic volume with the incoming wave arriving at the azimuth and elevation angles of θ and ϕ, respectively.

2 Cubic Array Formulation

Fig. 1 shows the placement of the receiving antenna elements on the cubic volume. There are a total of $N_1 \times N_2 \times N_3$ elements located on three perpendicular (x, y, z) directions. The distances between the elements along these directions are d_1, d_2 and d_3, respectively. The incoming wave arrives with the azimuth and elevation angles of $0 < \theta < 360°$ and $-90° < \phi < 90°$, respectively. The received signal at the array reaches the sample element (n_1, n_2, n_3), for $0 \leq n_1 \leq N_1 - 1$, $0 \leq n_2 \leq N_2 - 1$ and $0 \leq n_3 \leq N_3 - 1$, with a time delay that can be calculated as:

$$\tau(n_1, n_2, n_3) = \frac{1}{c}\Big[d_1 n_1 \cos\theta \sin\phi + d_2 n_2 \sin\theta \sin\phi + d_3 n_3 \cos\phi\Big] \qquad (1)$$

Equation (1) has been calculated with respect to the reference element $(0,0,0)$ and c is the speed of propagation. The frequency dependent phase angle at the location of the element (n_1, n_2, n_3) will be calculated as follows:

$$\phi(n_1, n_2, n_3) = 2\pi f \tau(n_1, n_2, n_3) \tag{2}$$

The signal received at each element is multiplied by $C_{n_1 n_2 n_3}$ and the overall transfer function in terms of angle and frequency can be written as:

$$H(f,\theta,\phi)=\sum_{n_1=0}^{N_1-1}\sum_{n_2=0}^{N_2-1}\sum_{n_3=0}^{N_3-1} C_{n_1 n_2 n_3} e^{j\frac{2\pi f}{c}(d_1 n_1 \cos\theta \sin\phi + d_2 n_2 \sin\theta \sin\phi + d_3 n_3 \cos\phi)} \tag{3}$$

For simplicity of analysis, three different frequencies are defined as:

$$f_1 = \frac{f d_1}{c}\cos\theta\sin\phi, \quad f_2 = \frac{f d_2}{c}\sin\theta\sin\phi, \quad f_3 = \frac{f d_3}{c}\cos\phi \tag{4}$$

which simplifies (3) to the following form:

$$H(f_1, f_2, f_3) = \sum_{n_1=0}^{N_1-1}\sum_{n_2=0}^{N_2-1}\sum_{n_3=0}^{N_3-1} C_{n_1 n_2 n_3} e^{j2\pi(n_1 f_1 + n_2 f_2 + n_3 f_3)} \tag{5}$$

The three dimensional frequency volume (f_1, f_2, f_3) is limited for f_1, f_2 and f_3 to $(-0.5, 0.5)$, because

$$|f_1| = \left|\frac{f d_1}{c}\cos\theta\sin\phi\right| \le \frac{f d_1}{c} \le \frac{f}{c}\frac{\lambda_{\min}}{2} = \frac{f}{c}\frac{c}{2 f_h} \le 0.5 \tag{6}$$

$$|f_2| = \left|\frac{f d_2}{c}\sin\theta\sin\phi\right| \le \frac{f d_2}{c} \le \frac{f}{c}\frac{\lambda_{\min}}{2} = \frac{f}{c}\frac{c}{2 f_h} \le 0.5 \tag{7}$$

$$|f_3| = \left|\frac{f d_3}{c}\cos\phi\right| \le \frac{f d_3}{c} \le \frac{f}{c}\frac{\lambda_{\min}}{2} = \frac{f}{c}\frac{c}{2 f_h} \le 0.5 \tag{8}$$

where, $\lambda_{\min}$ is the wavelength corresponding to the highest frequency f_h, and as a sensible choice we assume that the inter-element spacing is limited to the half of the lowest wavelength of the spectrum.

3 Calculations of Coefficients

For the calculation of the real coefficients $C_{n_1 n_2 n_3}$, we start with considering $L \ge 2$ focal points symmetrically located on the three dimensional space

generated by (f_1, f_2, f_3). These points do not include the origin. Then, two vectors, both with the length of L, are defined as follows:

$$\mathbf{b} = \left[b_1, b_2, \ldots, b_L\right]^T \tag{9}$$

$$\mathbf{H_0} = \left[H(f_{1_{0_1}}, f_{2_{0_1}}, f_{3_{0_1}}), \ldots, H(f_{1_{0_L}}, f_{2_{0_L}}, f_{3_{0_L}})\right]^T \tag{10}$$

where, the superscript ^{T} stands for transpose. The elements of the vector $\mathbf{H_0}$ have the same values for any two pairs $(f_{1_{0_l}}, f_{2_{0_l}}, f_{3_{0_l}})$, $l = 1, 2, \ldots, L$ which are symmetrical with respect to the origin of the (f_1, f_2, f_3) space. The vector $\mathbf{b}$ is an auxiliary vector and will be computed in the design process. Now, assume that $H(f_1, f_2, f_3)$ is expressed by the multiplication of three basic polynomials and then the summation of the weighted result by b_l as follows:

$$H(f_1, f_2, f_3) = \sum_{l=1}^{L} b_l \sum_{n_1=0}^{N_1-1} e^{j2\pi n_1 (f_1 - f_{1_{0_l}})} \sum_{n_2=0}^{N_2-1} e^{j2\pi n_2 (f_2 - f_{2_{0_l}})} \sum_{n_3=0}^{N_3-1} e^{j2\pi n_3 (f_3 - f_{3_{0_l}})} \tag{11}$$

We notice that by using this form of $H(f_1, f_2, f_3)$, we have reduced the problem of direct computation of $N_1 N_2 N_3$ coefficients $C_{n_1 n_2 n_3}$ from a complicated system of $N_1 N_2 N_3$ equations to a new problem of solving only L equations, because normally we select $L << N_1 N_2 N_3$. Anyhow, our final task will be finding $C_{n_1 n_2 n_3}$ from b_l. We can obtain the relationship between b_l and $C_{n_1 n_2 n_3}$ be rearranging (11) as follows:

$$\begin{aligned} H(f_1, f_2, f_3) \;=\; & \sum_{n_1=0}^{N_1-1} \sum_{n_2=0}^{N_2-1} \sum_{n_3=0}^{N_3-1} \left\{ \sum_{l=1}^{L} b_l e^{-j2\pi n_1 f_{1_{0_l}}} e^{-j2\pi n_2 f_{2_{0_l}}} e^{-j2\pi n_3 f_{3_{0_l}}} \right\} \cdot \\ & e^{j2\pi n_1 f_1} e^{j2\pi n_2 f_2} e^{j2\pi n_3 f_3} \end{aligned} \tag{12}$$

Comparing with (5) yields

$$C_{n_1 n_2 n_3} = \sum_{l=1}^{L} b_l e^{-j2\pi n_1 f_{1_{0_l}}} e^{-j2\pi n_2 f_{2_{0_l}}} e^{-j2\pi n_3 f_{3_{0_l}}} \tag{13}$$

After calculation of $\mathbf{b}$, (13) provides a formula to determine all coefficients $C_{n_1 n_2 n_3}$. The computation of $\mathbf{b}$ is done using (11). For this purpose, we define an $L \times L$ matrix $\mathbf{A}$ with the elements a_{kl}, $1 \leq k, l \leq L$ as follows:

$$a_{kl} = \sum_{n_1=0}^{N_1-1} e^{j2\pi n_1 (f_{1_{0_k}} - f_{1_{0_l}})} \sum_{n_2=0}^{N_2-1} e^{j2\pi n_2 (f_{2_{0_k}} - f_{2_{0_l}})} \sum_{n_3=0}^{N_3-1} e^{j2\pi n_3 (f_{3_{0_k}} - f_{3_{0_l}})} \tag{14}$$

It should be noted that $\mathbf{A}$ is a dense matrix having elements as the product and sum of complex numbers with a modulus of unity. Hence, the condition number of $\mathbf{A}$, which is the ratio of the largest to the smallest singular value in the singular value decomposition of the matrix, should be investigated with the variation of L for stability of the algorithm.

First it is shown that a_{kl} is bounded:

$$\begin{aligned} |a_{kl}| &= \left| \sum_{n_1=0}^{N_1-1} e^{j2\pi n_1 (f_{1_{0_k}} - f_{1_{0_l}})} \right| \left| \sum_{n_2=0}^{N_2-1} e^{j2\pi n_2 (f_{2_{0_k}} - f_{2_{0_l}})} \right| \left| \sum_{n_3=0}^{N_3-1} e^{j2\pi n_3 (f_{3_{0_k}} - f_{3_{0_l}})} \right| \\ &\leq \sum_{n_1=0}^{N_1-1} \left| e^{j2\pi n_1 (f_{1_{0_k}} - f_{1_{0_l}})} \right| \sum_{n_2=0}^{N_2-1} \left| e^{j2\pi n_2 (f_{2_{0_k}} - f_{2_{0_l}})} \right| \sum_{n_3=0}^{N_3-1} \left| e^{j2\pi n_3 (f_{3_{0_k}} - f_{3_{0_l}})} \right| \\ &\leq N_1 N_2 N_3 \end{aligned} \tag{15}$$

The constant value of $a_{kl} = N_1 N_2 N_3$ appears on the diagonal of the symmetric matrix $\mathbf{A}$. All other entries of this matrix have a smaller magnitude than this constant as shown in (15). Although the proof of the non-singularity of $\mathbf{A}$ is not discussed here; however, we would like to report that we never encountered any unstable case during the simulations using different values of azimuth and elevation angles or different values of the number of antenna elements or the parameter L.

Now, we can use (9) and (10) to derive

$$\mathbf{H_0} = \mathbf{A}\mathbf{b} \tag{16}$$

Thus, $\mathbf{b}$ is obtained as follows:

$$\mathbf{b} = \mathbf{A}^{-1}\mathbf{H_0} \tag{17}$$

In (17) we have assumed that $\mathbf{A}$ is not singular, so that its inverse exists. The proof of the non-singularity of $\mathbf{A}$ is impossible or extremely difficult as the elements of this matrix are functions of the selection of the azimuth and elevation angles, the choice of L and the dimensions of the array N_1, N_2, N_3. Simulation results with several values of these parameters never showed any difficulty in the calculations. The final step will be to calculate $C_{n_1 n_2 n_3}$ from the formula in (13).

We now discuss the allocation of L points $(f_{1_{0_l}}, f_{2_{0_l}}, f_{3_{0_l}})$ with the corresponding values of $H(f_{1_{0_l}}, f_{2_{0_l}}, f_{3_{0_l}})$ in the (f_1, f_2, f_3) space. The simplest but non-trivial way to perform this allocation is $L = 2$. The selection of these two points should be appropriate in order to generate a set of real coefficients $C_{n_1 n_2 n_3}$. For this purpose, as shown in Fig. 2, we need to select

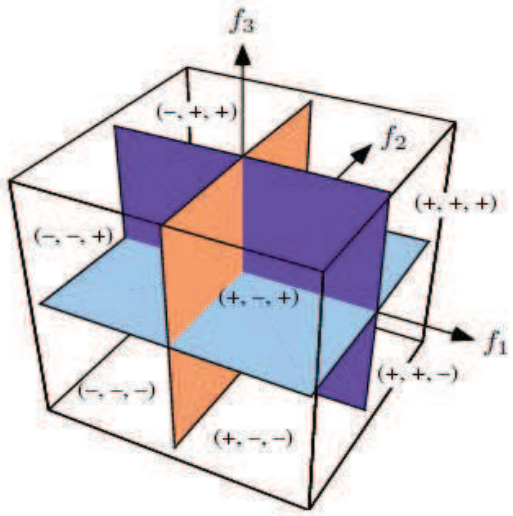

Figure 2: Space covered by (f_1, f_2, f_3) and different octants.

two points P_1 and P_2 symmetrically located in octant 1 and 7, ladled by $(+,+,+)$ and $(-,-,-)$, respectively.

$$\begin{aligned} P_1: &\quad (f_{1_{0_1}}, f_{2_{0_1}}, f_{3_{0_1}}) = (f_{1_0}, f_{2_0}, f_{3_0}) \\ P_2: &\quad (f_{1_{0_2}}, f_{2_{0_2}}, f_{3_{0_2}}) = (-f_{1_0}, -f_{2_0}, -f_{3_0}) \end{aligned} \tag{18}$$

Then, values at these points:

$$\mathbf{H_0} = [1, 1]^T \tag{19}$$

The symmetric selection guarantees that the coefficients are real and also that we have a unit gain at the desired point on the (f_1, f_2, f_3) space. More complex choices can be made by adding several symmetric zeros to (18). For example, we can apply permutation rule to $(\pm f_1, \pm f_2, \pm f_3)$ and increase the number of critical points to $L = 18$ as follows:

$$\begin{aligned} &(f_{1_0}, f_{2_0}, f_{3_0}), (-f_{1_0}, -f_{2_0}, -f_{3_0}), (f_{2_0}, f_{3_0}, -f_{1_0}), (-f_{2_0}, -f_{3_0}, f_{1_0}) \\ &(f_{2_0}, -f_{3_0}, f_{1_0}), (-f_{2_0}, f_{3_0}, -f_{1_0}), (f_{2_0}, -f_{3_0}, -f_{1_0}), (-f_{2_0}, f_{3_0}, f_{1_0}) \\ &(f_{2_0}, f_{3_0}, f_{1_0}), (-f_{2_0}, -f_{3_0}, -f_{1_0}), (f_{3_0}, f_{1_0}, -f_{2_0}), (-f_{3_0}, -f_{1_0}, -f_{2_0}) \\ &(-f_{3_0}, -f_{1_0}, f_{2_0}), (f_{3_0}, f_{1_0}, -f_{2_0}), (f_{3_0}, -f_{1_0}, -f_{2_0}), (-f_{3_0}, f_{1_0}, f_{2_0}) \\ &(f_{3_0}, f_{1_0}, f_{2_0}), (-f_{3_0}, -f_{1_0}, -f_{2_0}) \end{aligned} \tag{20}$$

For which we define:

$$\mathbf{H_0} = [1, 1, 0, 0, 0, 0, 0, 0, 0, 0, 0, 0, 0, 0, 0, 0, 0, 0]^T \tag{21}$$

That means the first two points P_1 and P_2 will be assigned an amplitude of one and the other 16 will have an amplitude of zero to improve the directivity of the resultant pattern.

The selection of L is voluntary, however, to assure real coefficients for array elements, L needs to be even. In order to complete the design with any other even values of L between 2 and 18 (which is the maximum number we can generate by permutation of $(\pm f_1, \pm f_2, \pm f_3)$) we only need to keep the first L values of (20) and discard the rest. Similarly, $\mathbf{H_0}$ in (21) will only have two ones and $L-2$ zeros.

4 Simulation Results

For the first simulation, we assume the simplest case of $L = 2$ as in (18) and (19). The array configuration consists of $4 \times 4 \times 4$ elements. The desired azimuth and elevation angles are $\theta = 70^\circ$ and $\phi = -50^\circ$. The lowest and highest operational frequencies have been considered as 3 GHz and 4 GHz, respectively. This will generate a fractional bandwidth of about 30%. We also assume that the inter-element spacing of the array is $d_1 = d_2 = d_3 =$ 3.75 cm, which is half wavelength of the highest frequency.

To assign the values of P_1 and P_2, we have to calculate $f_{1_0}, f_{2_0}, f_{3_0}$ from (4). Then, $\mathbf{A}$ is constructed using (14) and $\mathbf{b}$ is calculated from (17). Finally, the coefficients $C_{n_1 n_2 n_3}$, for $1 \leq n_1, n_2, n_3 \leq 4$, are computed from (13). Due to the symmetry of the selected points in the (f_1, f_2, f_3) space, the values of $C_{n_1 n_2 n_3}$ are all real which reduces the computation load considerably and the array system will be fully spatially processed.

Fig. 3 shows a normalized plot of $H(f_1, f_2, f_3)$ calculated from (11) as a function of f_1 and f_2 while f_3 is kept constant to its nominal value when calculated at the mid-range operational frequency. In the same way, Figs. 4 and 5 demonstrate the variation of $H(f_1, f_2, f_3)$ as f_2 and f_1, respectively, are maintained at their nominal values. All three figures show a relatively smooth variation of the magnitude close to the selected points based on (18). These mild variations are the key reasons for the frequency independence of the designed array, particularly near the desired direction.

Directional patterns of the three dimensional array with frequency variations from 3 GHz to 4 GHz are shown in Figs. 6 and 7 for azimuth and elevation angles, respectively. Both figures show the frequency independence of the design within the range and for the main lobe of the pattern. Relatively more variations are observed for the sidelobes but they all are happening below 10 dB attenuation.

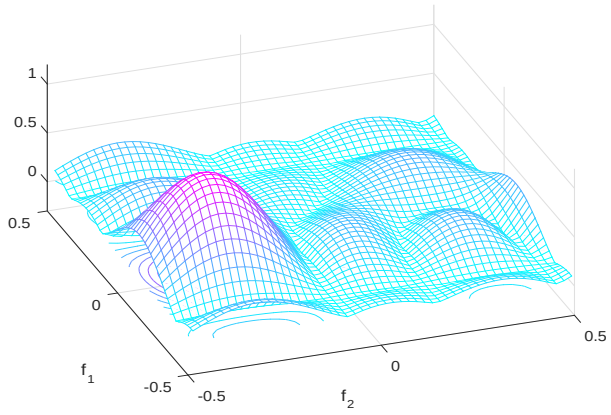

Figure 3: Normalized plot of $H(f_1, f_2, f_3)$ as a function of f_1 and f_2. The global maximum is located at $(f_1 = -0.1146, f_2 = -0.3149)$.

Further simulations show that increasing $L = 2$ to $L = 18$ and using (20) together with (21) will decrease the beamwidth, sidelobe levels and frequency dependence by different factors that can be as high as 60% for sidelobes. These observations are presented in Figs. 8 and 9. As we can notice, the 10 dB beamwidth has improved from 71° to 59° for the azimuth and from 52° to 45° for the elevation. This improvement is higher for the sidelobe attenuation levels which reduces from -12 dB to -20 dB.

For a comparison between the proposed algorithm and other methods employing cubic array structures, we have simulated the beamforming designs for the same number of elements and similar azimuth and elevation angles using the Fourier transform technique described in [1] and [9] for calculation the weights connected to each element. The result of simulation is demonstrated in Figs. 10 and 11 for azimuth and elevation angles, respectively. These figures show that the sidelobe levels are only 6-8 dB lower than the main lobe, as compared to the 12-20 dB of the propose method in Figs. 6 to 9.

The second comparison is between the proposed method and the LMS adaptive algorithm for calculation of the real-valued coefficients. The LMS algorithm uses the following equation:

$$C_{n_1 n_2 n_3}(t + \delta t) = C_{n_1 n_2 n_3}(t) + \mu e(t) s_{n_1 n_2 n_3}(t) \tag{22}$$

to direct the mean squared error (MSE) toward zero, where μ is the step size or convergence factor and controls the convergence speed and stability

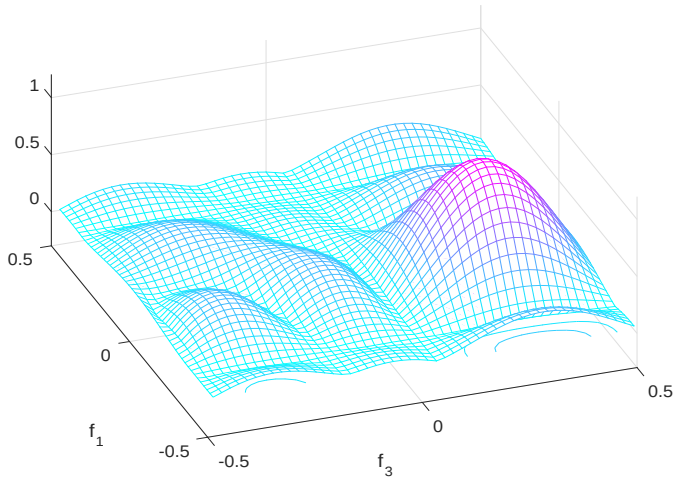

Figure 4: Normalized plot of $H(f_1, f_2, f_3)$ as a function of f_1 and f_3. The global maximum is located at $(f_1 = -0.1146, f_3 = 0.2812)$.

of the calculations, $s_{n_1 n_2 n_3}(t)$ is the input signal and δt is the time interval between two successive iterations. The result of simulation is demonstrated in Figs. 12 and 13 for azimuth and elevation angles, respectively. As it is observed, the results are not as good as the case of $L = 2$ in Figs. 6 and 7 or the case of $L = 18$ in Figs. 8 and 9 for sidelobe levels, 10 dB beamwidth and frequency independence.

Finally, to investigate the frequency range and bandwidth dependency of the proposed algorithm, Figs. 6 and 7 for azimuth and elevation angles of $\theta = 70^\circ$ and $\phi = -50^\circ$, respectively, have been repeated for a higher and wider frequency range of 7.5 GHz to 10 GHz which is the higher portion of the ultra wideband (UWB) technology spectrum mask with a fractional bandwidth of about 30%. The results are shown in Figs. 14 and 15, respectively. As we can see, as long as the fractional bandwidth is kept constant, the performance of the designed beamformimg is basically the same across the whole UWB frequency domain.

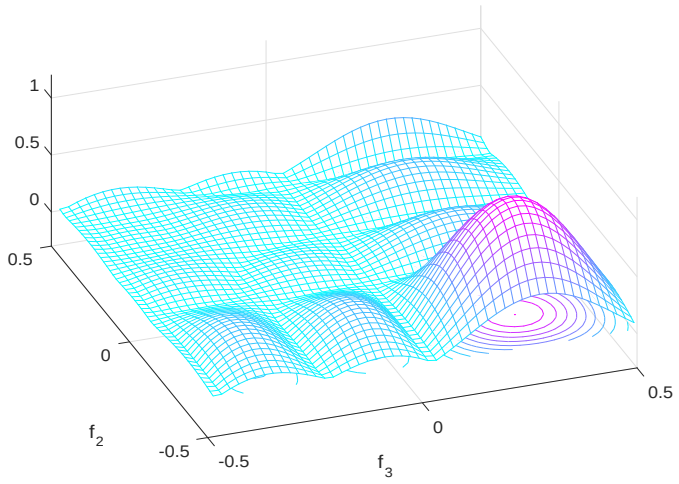

Figure 5: Normalized plot of $H(f_1, f_2, f_3)$ as a function of f_2 and f_3. The global maximum is located at $(f_2 = -0.3149, f_3 = 0.2812)$.

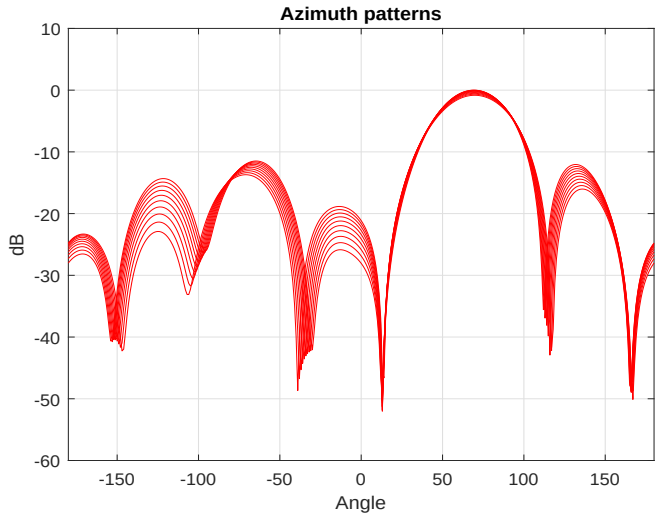

Figure 6: Azimuth patterns for 3-4 GHz with the desired value of $\theta = 70°$ when $L = 2$.

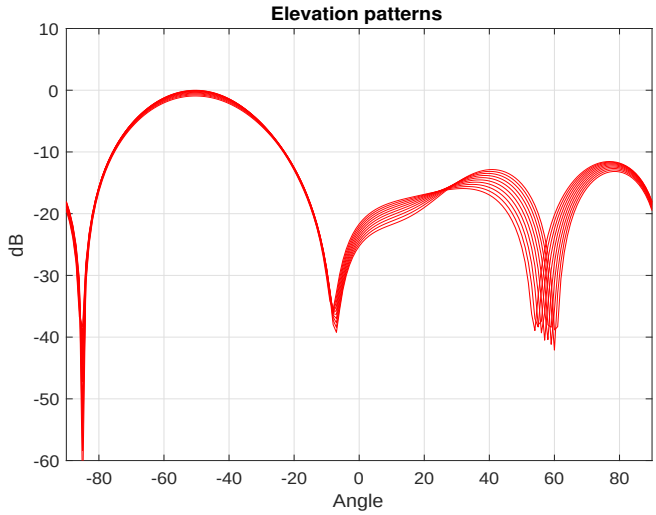

Figure 7: Elevation patterns for 3-4 GHz with the desired value of $\phi = -50°$ when $L = 2$.

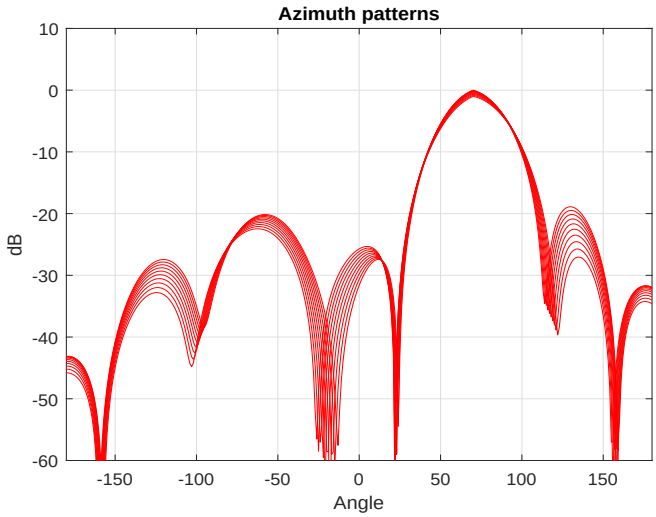

Figure 8: Azimuth patterns for 3-4 GHz with the desired value of $\theta = 70°$ when $L = 18$.

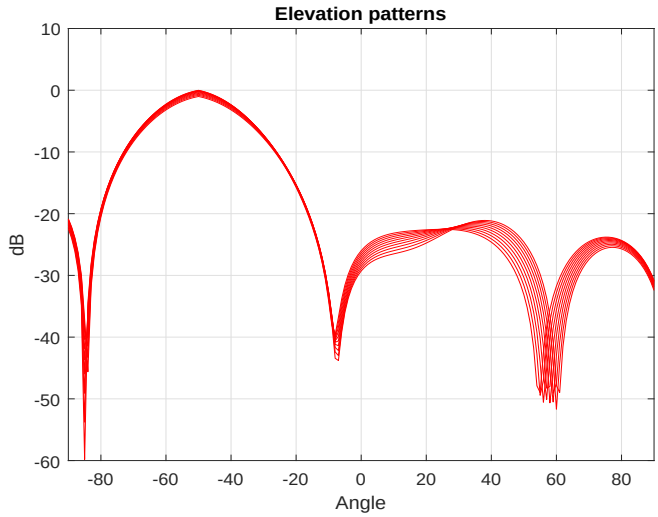

Figure 9: Elevation patterns for 3-4 GHz with the desired value of $\phi = -50°$ when $L = 18$.

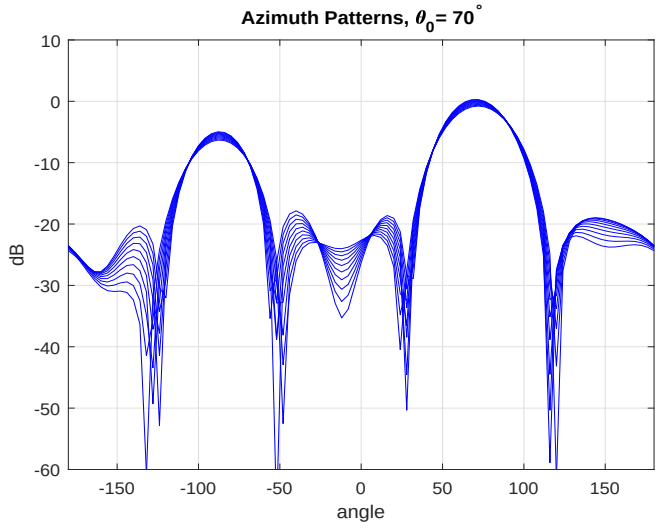

Figure 10: Azimuth patterns for 3-4 GHz with the desired value of $\theta = 70°$ using Fourier transform algorithm.

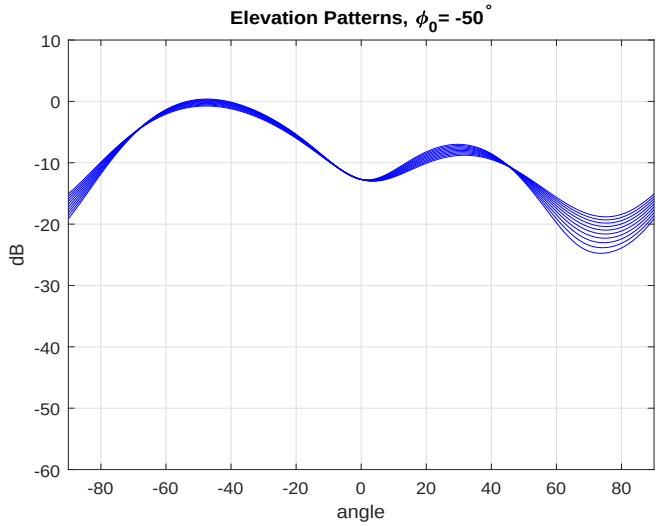

Figure 11: Elevation patterns for 3-4 GHz with the desired value of $\phi = -50°$ using Fourier transform algorithm.

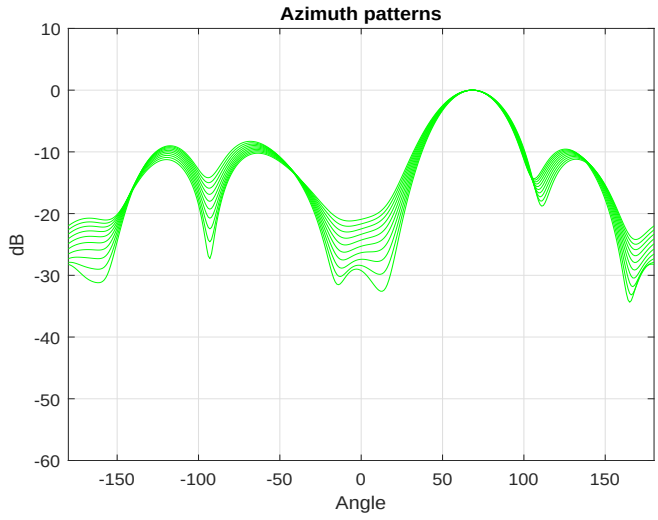

Figure 12: Azimuth patterns for 3-4 GHz with the desired value of $\theta = 70°$ using LMS algorithm.

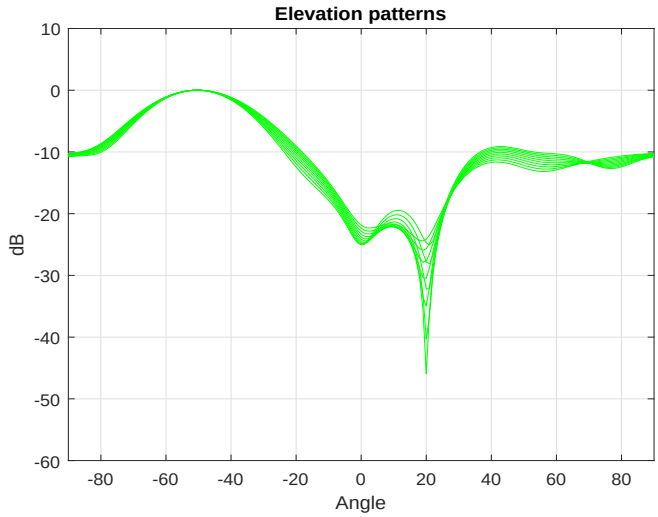

Figure 13: Elevation patterns for 3-4 GHz with the desired value of $\phi = -50°$ using LMS algorithm.

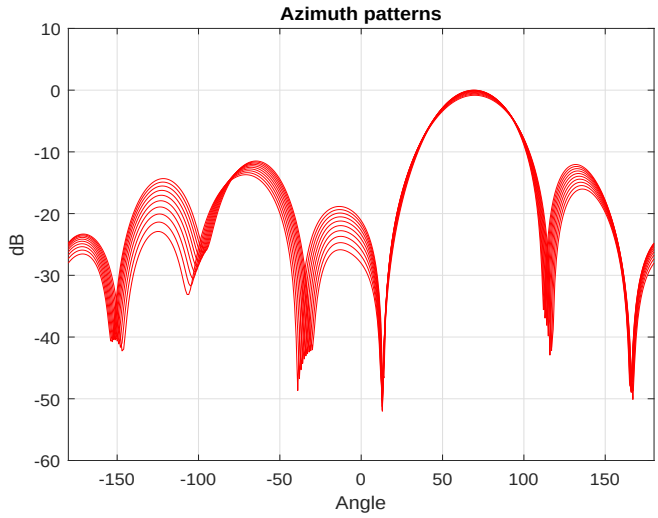

Figure 14: Azimuth patterns for 7.5-10 GHz with the desired value of $\theta = 70°$ when $L = 2$.

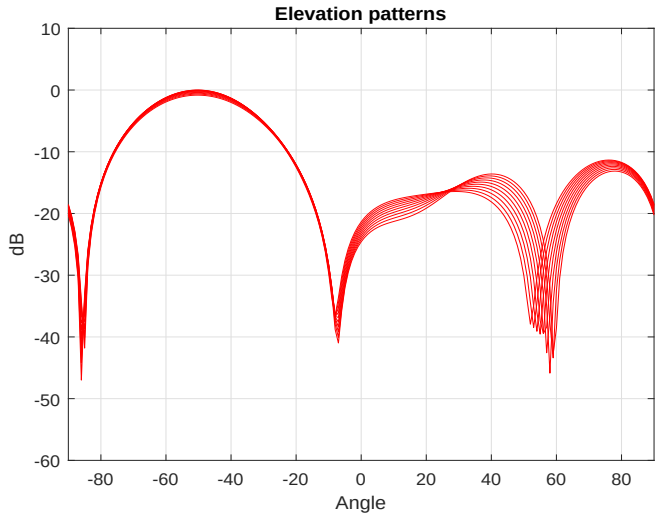

Figure 15: Elevation patterns for 7.5-10 GHz with the desired value of $\phi = -50^\circ$ when $L = 2$.

5 Conclusions

A simple method for the design of a cubic array system with a real-valued multiplier for each antenna element was presented. The fully spatial beamformer can steer the beam toward both azimuth and elevation directions covering the whole three dimensional space. The configuration benefits from the frequency invariance of the patterns within a relatively large fractional bandwidth of about 30%, which may be used in the whole UWB spectrum for different applications. The real multipliers were calculated based on matrix manipulation methods. However, the dimension of the matrices and vectors used in the computations can be much lower than the total number of antenna elements. Simulation results show that, even with the minimum number of required focal points ($L = 2$), the designed array shows an appropriate level of directivity and frequency independence for a fractional bandwidth of 30% within the UWB spectral mask from 3 to 10 GHz. Moreover, a comparison was made with the Fourier transform based and adaptive LMS algorithm methods in terms of the directivity and sidelobe levels to show the advantages of the proposed algorithm.

References

[1] W. Liu, *Wideband Beamforming Concepts and Techniques*, John Wiley & Sons, UK, 2010.

[2] L. Liang and S. V. Hum, "Experimental characterization of UWB beamformers based on multidimensional beam filters", *IEEE Trans. Antenna and Propagation*, vol. 59, no. 9, pp. 304-309, Jan. 2011.

[3] M. Hawes and W. Liu, "Sparse array design for wideband beamforming with reduced complexity in tapped delay-lines", *IEEE Trans. Audio, Speech, and Lang. Proc.*, vol. 22, no. 8, pp. 1236-1247, Aug. 2014.

[4] B. Allen and M. Ghavami, *Adaptive Array Systems: Fundamentals and Applications*, John Wiley & Sons, 2005.

[5] M. Ghavami, "Wideband smart antenna theory using rectangular array structures", *IEEE Trans. Sig. Proc.*, vol. 50, no. 9, pp. 2143-2150, Sep. 2002.

[6] D. Overturf, K. Buchanan, J. Jensen, C. Flores-Molina, S. Wheeland and G. H. Huff, "Investigation of beamforming patterns from volumet-

rically distributed phased arrays," in Proc. IEEE Military Communications Conference (MILCOM), pp. 817-822, Oct. 2017.

[7] S. Srikanth, N. S. Chaya, S. Gurugopinath and K. George, "Optimal detection of a particle source using cubical and spherical directional detector arrays," in Proc. American Control Conference (ACC), May 2017.

[8] Y. Q. Zhao, Z. Peng, "Three-dimensional phased array antenna analysis and simulation," in Proc. IEEE International Symposium on Microwave, Antenna, Propagation and EMC Technologies for Wireless Communications, Oct. 2009.

[9] W. Liu and S. Weiss, *Design of Frequency Invariant Beamformers for Broadband Arrays*, IEEE Transactions on Signal Processing, vol. 56, no. 2, pp. 855-860, Feb. 2008.

[10] J. Garza, M. A. Panduro, A. Reyna, A. Mendez, and D. H. Covarrubias, "Design of 3D cubic antenna arrays with low side lobe level during beam-scanning," in Proc. Asia-Pacific Conference on Antennas and Propagation, Jul. 2016.

[11] B. Widrow S. D. Stearns, *Adaptive Signal Processing*, Prentice-Hall, Englewood Cliffs, N.J., 1985.